Japanese Journal of Radiology (2019) 37:694–700
https://doi.org/10.1007/s11604-019-00862-y

ORIGINAL ARTICLE

Whole-tumor histogram analysis of DWI and QSI for differentiating between meningioma and schwannoma: a pilot study

Hitomi Nagano[1] · Koji Sakai[1] · Jun Tazoe[1] · Masashi Yasuike[1] · Kentaro Akazawa[1] · Kei Yamada[1]

Received: 7 May 2019 / Accepted: 30 July 2019 / Published online: 8 August 2019

Abstract

Purpose To investigate whether whole-tumor histogram analyses of diffusivity measurements derived from q-space imaging (QSI) improves the differentiation between meningioma and schwannoma.

Materials and methods Fifteen extra-axial tumors (11 meningiomas and 4 schwannomas) with MR examinations from April 2011 to May 2013 were included. Three-dimensional regions of interest (ROI) encompassed the whole tumor, including cystic areas. Histogram analyses of mean displacement (MD) derived from QSI and apparent diffusion coefficient (ADC) for the ROI were performed at mean, the five percentiles of MD_n and ADC_n ($n = 5$, 25, 50, 75, 95th), kurtosis, and skewness. To determine the diagnostic ability of MD_n and ADC_n, we also compared the area under the curve (AUC) on receiver operating characteristic (ROC) analysis.

Results Histogram analyses revealed significant differences between meningioma and schwannoma in MD_{75}, ADC_{25}, ADC_{50}, ADC_{75}, and kurtosis of ADC. The ROC analysis of kurtosis of ADC and MD_{75} resulted in an AUC of 1.0 and 0.96, respectively. There were no significant differences between the AUC of MD_{75} and that of kurtosis of ADC ($p = 0.41$).

Conclusion The histogram analyses of MD and ADC derived from QSI were both equally useful in differentiating between intracranial meningioma and schwannoma.

Keywords Schwannoma · Meningioma · Magnetic resonance image (MRI) · Q-space image (QSI) · Diffusion-weighted image (DWI)

Introduction

Meningioma and schwannoma are the two most frequently observed extra-axial brain tumor types. Surgical approaches for these entities are vastly different [1–4]; thus, the preoperative differentiation between these two conditions is important. However, when one encounters a tumor at the cerebellopontine angle (CPA), for example, discrimination between these entities can be sometimes a diagnostic challenge [5, 6]. There are many helpful morphologic characteristics on magnetic resonance (MR) imaging, but some cases present with very similar characteristics [5–9]. Thus, more objective measures that aid in diagnosis can be of clinical value.

Diffusion-weighted imaging (DWI) has been shown to be a reliable tool that quantifies the movement of water molecules and has been used for differentiating between meningioma and schwannoma [10–12]. This method is thought to be effective due to the differences in tumoral microstructure and/or cell density between them.

Q-space imaging (QSI) is a more advanced MR imaging method that enables the estimation of non-Gaussian diffusion, providing another way to assess the tissues [13]. Whereas the DWI depicts the average migration distances of water molecules, QSI provides more detailed information of tissue microstructures using multiple high b values. This information can be derived from the mean displacement (MD) of QSI [14]. It has been reported that QSI has higher sensitivity in detecting pathological information for several benign brain lesions [15–18], but only few studies have reported on its application to tumors [19–22]. Moreover,

✉ Koji Sakai
sakai3@koto.kpu-m.ac.jp

[1] Department of Radiology, Graduate School of Medical Science, Kyoto Prefectural University of Medicine, 465 Kajii-cho, Kawaramachi Hirokoji Sagaru, Kamigyo-ku, Kyoto 602-8566, Kyoto, Japan

there have been no reports regarding QSI for differentiating between meningioma and schwannoma.

Regions-of-interest (ROI) analysis is a commonly utilized technique in analyzing medical images. A few comparatively simple types of data can be derived from ROI analysis, such as mean, minimum, and maximum values. Many of the previous studies have chosen to place ROIs only over the solid components of the tumor by carefully avoiding any cystic or hemorrhagic regions within the tumor [10–12]. This was done with the notion that using ROIs covering these heterogeneous components will lead to less accurate information about the tumoral properties [23, 24]. However, such techniques have the potential for bias in the way of placing the ROI. In addition, manual selection of solid component is a time-consuming process.

Histogram analysis is a method that has become popular in the field of medical imaging over the past few years. It enables handling continuous data of the whole region and will provide multiple evaluation methods through descriptive statistics including percentile, kurtosis, and skewness. It is expected to represent the tissue microstructures and their detailed distribution, leading to better reflecting the histological characteristics of the tumors [23].

In this study, we tested the ability of DWI and QSI in differentiating between intracranial meningioma and schwannoma, using histogram analysis in three-dimensional (3D) ROIs that cover the whole tumor.

Materials and methods

Subjects

This retrospective study was approved by our institutional review board. This is an opt-out research design and all opportunities for the patients were provided to them through publicly posted notifications. Thirteen patients with a meningioma and 5 patients with a schwannoma underwent MR examination from April 2011 to May 2013 in our hospital, all of which included QSI sequences. Two patients with a meningioma and one patient with a schwannoma were excluded due to the absence of pathological examination, and one patient with a schwannoma was excluded due to technically inadequate image quality. After these exclusions, 11 patients with a meningioma and 4 patients with a schwannoma were finally included in this pilot study.

All tumors were located intracranially and the locations of the meningiomas were CPA ($n=4$), parasagittal ($n=3$), convexity ($n=2$), and falcine ($n=2$). The locations of the schwannomas were CPA ($n=3$) and trigeminal ($n=2$). All 11 meningiomas and 4 schwannomas were pathologically diagnosed following total or partial resection. Using the World Health Organization classification system, the subtypes of meningioma were determined by a pathologist to be, transitional ($n=6$), fibrous ($n=2$), mixed ($n=1$), psammomatous ($n=1$), or atypical ($n=1$).

Data acquisition

All MR examinations were performed using a 1.5-T whole-body imager (Philips Medical Systems, Best, The Netherlands). In all MR scans, the field of view was 23 × 23 cm. DWI for QSI was acquired using a single-shot, echo-planar imaging technique with repetition time (TR)/echo time (TE) = 6000/173 ms, duration between the paired gradients (Δ)/time of applied gradient (δ) = 142/17 ms, effective diffusion time (T_{diff}) = 136 ms, defined here as Δ-(δ/3), and a matrix of 128 × 128, without cardiac gating. Gradient magnitudes were increased in nine steps to reach a maximal b value of 10,000 s/mm^2 and a maximal q value of 855/cm (the q value is derived from b value by $q = b/\{4\pi^2(\Delta - \delta/3)\}$). The b values used were 0, 10, 60, 100, 300, 600, 1000, 3000, 6000, and 10,000 s/mm^2. Motion-sensitizing gradients were applied in 15 directions. A total of twelve 3-mm-thick sections were obtained without intersection gaps to cover the whole tumor. These DWIs were motion/distortion corrected to match the $b=0$ images on the console of the MR unit. The q-space data set included 136 images per slice (nine diffusion images in 15 diffusion gradient directions) with a total acquisition time of 25 min.

Data post-processing and analysis

Data were sent to an offline computer for further analysis on the in-house software (written in Matlab® code). The q-space analysis was performed on a pixel-by-pixel basis, as previously described [25]. High b value components above 10,000 s/mm^2 were zero-filled upon analysis. First, the mean displacement (MD) distribution profile was calculated for each gradient direction by Fourier transformation of the signal decay. The full-width at half-maximum of the displacement distribution profile was then calculated, and these values were used to represent the MD. The ADC maps were created using the $b=0$ and $b=1000$ s/mm^2 images of QSI.

ROIs encompassing the whole volume of each tumor on $b=0$ images or DWI images were applied using the ImageJ software (https://rsb.info.nih.gov/ij/) and Fiji (https://fiji.sc). ROIs were traced slightly smaller than the margins of the whole lesion to avoid a partial volume effect and any portions invasive into the skull, with reference to the corresponding T2-weighted and contrast-enhanced T1-weighted images (CET1WI). The ROIs were defined for each lesion by a single board-certified radiologist with 11 years of experience.

Histogram analyses were performed for each ROI. The histogram measures included the mean and five measures:

the 5th, 25th, 50th (median), 75th, and 95th percentiles (MD_n, ADC_n). The *n*th percentile is the point at which *n* percent of the voxel values that form the histogram are found to the left. The kurtosis and skewness of histogram were also calculated. Kurtosis reflects the peakedness of the distribution and is a measure of the shape of a probability distribution. Skewness represents a measure of asymmetry of the probability distribution. These percentiles, the kurtosis, and the skewness represent statistical properties of heterogeneity in the region of tumor.

Statistics

All continuous variables of the histogram parameters proved to have a non-normal distribution (Kolmogorov–Smirnov test). The difference of patients' sex between patients with meningioma and schwannoma was compared using the Fisher's exact test. The Mann–Whitney *U* test was used to test differences of patient age and tumor volume between two groups for continuous variables. The tumor volume was derived from whole-volume ROI. The histograms for the sum of our cases were plotted placing meningiomas beside schwannomas in MD and ADC values. The optimal number of bins was determined by Scott's rule. We assessed the similarity of the histogram curve between MD and ADC values of the sum of our cases using a two-sample Kolmogorov–Smirnov test, with p value < 0.05 as significant. The mean and seven histogram measures between the two groups were tested with the Mann–Whitney *U* test for continuous variables. For these eight measures, Bonferroni correction was used for multiple comparisons. Therefore, p value < 0.00625 (0.05/8) was considered to indicate a statistically significant difference [26]. To determine the diagnostic ability of QSI, receiver operating characteristic (ROC) analyses were performed for the histogram measures. The cut-off values were determined by maximizing the sum of sensitivity and specificity (Youden index) [27]. We performed DeLong's test [28], with $p < 0.05$ as significant, to determine the differences between MD and ADC with the highest area under the curve (AUC).

All statistical analyses were performed with R (The R Foundation for Statistical Computing, Vienna, Austria, version 3.2.1) and EZR (Saitama Medical Center, Jichi Medical University, Saitama, Japan), which is a graphical user interface for R [29].

Results

There was no statistically significant difference among patient age, sex, and tumor volume between meningioma and schwannoma, as shown in Table 1. Representative cases of meningioma and schwannoma are presented in Fig. 1.

Table 1 Demographic data

Parameter	Meningioma	Schwannoma	*p* value
Patients (*n*)	11	4	
Age, years	60.0	59.5	0.65
Patient sex			0.06
Male	1	2	
Female	11	2	
Tumor volume (cm^3)	12.0	4.7	0.28

p value < 0.05 as significant difference

The values except p value in age and tumor volume were median

Figure 2 shows the histograms of meningioma and schwannoma for the sum of our cases, for which distribution patterns were significantly different between the histograms of MD and ADC ($p < 0.05$). Table 2 shows the comparison of histogram measures between meningioma and schwannoma. Significant differences were found in the following measures: MD_{75} and ADC_{25}, ADC_{50}, ADC_{75}, and the kurtosis of ADC. Schwannomas showed significantly higher MD and ADC values than meningiomas. The kurtosis of ADC had the best AUC among all histogram measures (AUC = 1.0). MD_{75} had the best AUC among histogram measures of MD (AUC = 0.96) (Table 3). Although the AUC of kurtosis of ADC was higher than those of MD_{75} and ADC_{75}, there were no significant differences in ROC analysis between kurtosis of ADC and MD_{75} ($p = 0.41$) (Fig. 3).

Discussion

Histogram analysis is known to be an effective way of assessing the tissue properties of various lesions, including brain tumors [12, 30–32]. We have shown in this study that differentiation between meningioma and schwannoma is possible using histogram analysis of the diffusivity derived from DWI and QSI using a targeted 3D-ROI that covers the whole-tumor region.

A previous study using DWI with ROI over the solid component reported that the best differentiating ability was observed at the 90th percentile of ADC [12] and our results concur with this study. As shown in Table 2, among the mean and seven histogram measurements obtained for ADC, four allowed for good discrimination, including kurtosis, and the 25th, 50th, and 75th percentiles. On the other hand, QSI showed that a single measurement, the 75th percentile of MD, had good discrimination between the two entities. There was, however, no substantial difference in the diagnostic power between ADC and MD, as shown in Fig. 3.

The distribution patterns of the histograms for all cases are shown in Fig. 2, and these further support the significant difference in diffusion properties between meningioma and

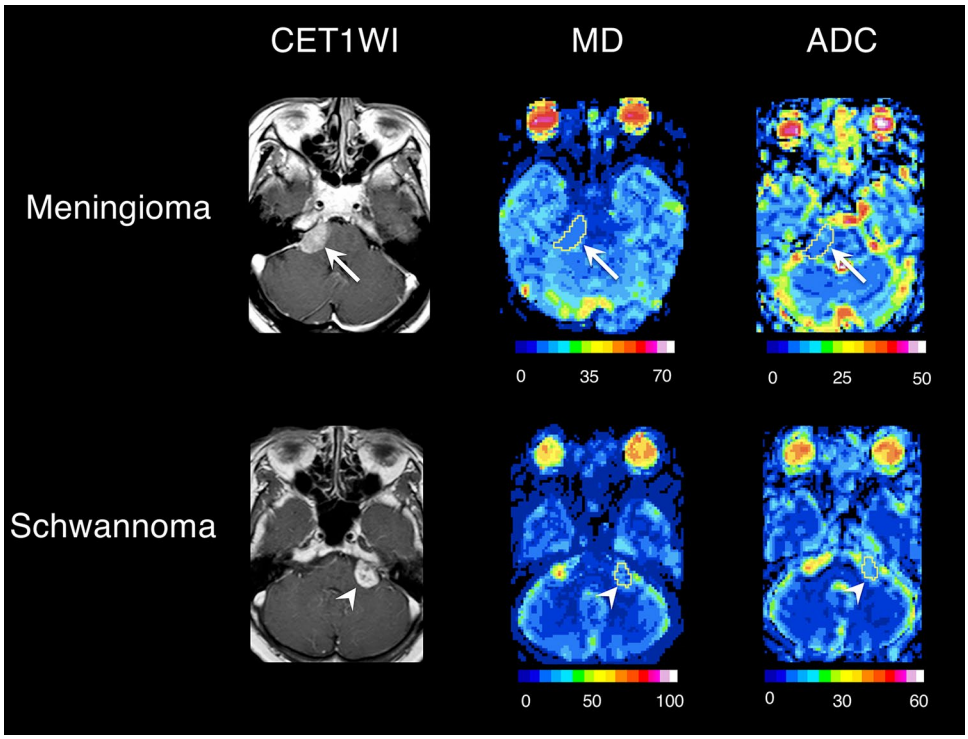

Fig. 1 Representative cases of meningioma and schwannoma. CET1WI contrast-enhanced T1-weighted images, MD mean displacement, ADC apparent diffusion coefficient. The upper row shows a meningioma (arrow) in a 60-year-old woman and the lower row shows a schwannoma (arrow head) in a 62-year-old woman. MD maps derived from QSI and ADC maps derived from $b=0$ and $b=1000$ images were overlaid by the ROI. MD values are given in units of μm and ADC values are given in units of $10^{-3} \times mm^2/s$ in mean and percentiles

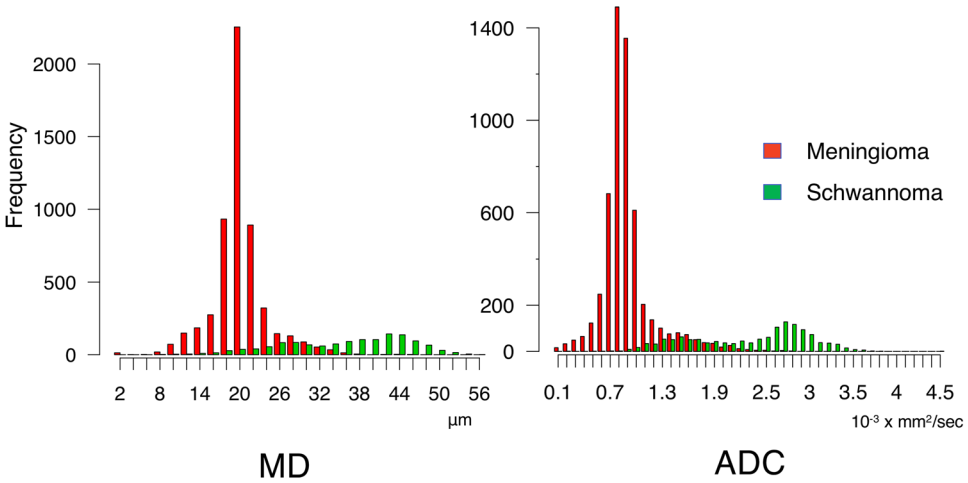

Fig. 2 Histograms of MD derived from QSI and ADC for all cumulative cases using the sum of our cases. *MD* mean displacement, *ADC* apparent diffusion coefficient. Red histograms show meningioma and green histograms show schwannoma

schwannoma. The histogram of schwannoma showed higher frequency in the bins of large values for both MD and ADC compared to that of meningioma.

The statistical difference in diffusion properties between the two tumors can be attributable to differences in histological structures. It is well known that there is a two-cell-pattern histology for schwannoma with high (Antoni A) and low (Antoni B) cell densities [10–12]. The higher mean ADC and MD values in schwannoma are considered to reflect the presence of low-cell-density tissues.

Many of the previous studies have used manual ROI placement only on the solid components [10, 11]. One of these studies not only avoided placing ROIs on hemorrhagic areas within the schwannomas, but also even excluded cases with cyst formation [12]. We employed a more objective and feasible method of placing the ROI than those in the previous reports while still achieving similar results.

We initially hypothesized that utilizing whole-tumor ROIs might lead to substantially higher mean ADC values for schwannomas, as they tend to be more frequently cystic than meningiomas [5, 6]. Contrary to this expectation, the mean ADC values did not differ significantly between the two entities, and this may be due to the fact that some of the meningiomas had areas with high ADC, probably representing microcystic components [11].

Table 2 Histogram analyses of MD and ADC

Histogram measures	MD			ADC		
	Meningioma	Schwannoma	*p* value	Meningioma	Schwannoma	*p* value
Mean	19.4	24.2	0.01	0.83	1.41	0.01
5th	14.2	16.6	0.67	0.55	0.99	0.03
25th	17.5	21.1	0.23	0.71	1.23	0.0058*
50th	18.8	25.1	0.01	0.83	1.41	0.0058*
75th	20.6	29.6	0.0059*	0.9	1.61	0.0029*
95th	23.7	33.5	0.01	1.27	1.95	0.06
Skewness	0.67	− 0.62	0.01	1.04	− 0.28	0.01
Kurtosis	3.2	− 0.05	0.02	2.36	− 0.35	0.0015*

MD values are given in units of μm and ADC values are given in units of $10^{-3} \times mm^2/s$ in mean and percentiles

MD mean displacement, *ADC* apparent diffusion coefficient, *n*th the *n*th percentile

*p value < 0.00625, significant difference after Bonferroni correction for multiple comparisons

All values except p value were median

Table 3 ROC analysis

Histogram measures	AUC	95% CI	Cut-off value	Sensitivity	Specificity
75th MD	0.96	0.85–1	26.5	0.91	1
25th ADC	0.96	0.85–1	0.88	0.91	1
50th ADC	0.96	0.85–1	1.32	0.91	1
75th ADC	0.98	0.91–1	1.51	0.91	1
Kurtosis of ADC	1	1–1	0.50	1	1

MD mean displacement, *ADC* apparent diffusion coefficient, *n*th *n*th percentile, *AUC* area under the curve, *CI* confidence interval

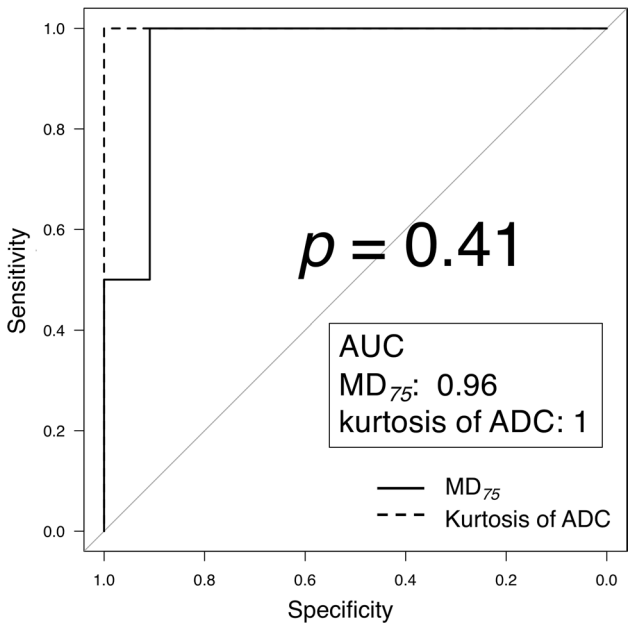

Fig. 3 ROC curves of the 75th percentiles MD (MD_{75}) and the kurtosis of ADC. *MD* mean displacement, *ADC* apparent diffusion coefficient. There was no significant difference between these AUC

QSI is an advanced MR imaging technique that has been shown to be superior to DWI in discriminating several diseases, such as cerebral ischemia, multiple sclerosis, and small vessel disease, among others [15–18]. Although the distribution of MD and ADC, as shown in Fig. 2, had statistically significant difference ($p < 0.05$, two-sample Kolmogorov–Smirnov test), the degree of difference seemed to be a very subtle one. As stated earlier, DWI and QSI are both able to assess the tumoral properties noninvasively. They will be able to assess the tumoral cellularity as well as internal microstructures within the cells [20]. Our results have shown that these factors can be equally well depicted using both imaging techniques. QSI, however, takes much longer acquisition time. This makes it difficult to be used in routine clinical setting. We are currently working on a few different ways to shorten the acquisition time of QSI [33]. This may lead to the routine use of this technique, but with the current form, we believe that there is a very little benefit in applying QSI to differentiate between benign tumors.

There are some other limitations in this study. First, the number of the cases are small. Second, the locations of meningioma included in this study were situated not only at

CPA, but also at various other regions. Third, the ADC values were calculated from $b=0$ and $b=1000$ s/mm^2 of QSI, which has slightly longer effective diffusion time (136 ms) than that conventionally employed (typically 50–80 ms). We chose to use this DWI to avoid registration errors of ROI. If we chose to use the conventional DWI, obtained separately, for ADC calculations, separate ROI placements would be necessary. This would likely lead to substantial differences in the size and shape of the ROIs, as there will be different degrees of image distortion, especially problematic for the posterior fossa. Finally, other types of extra-axial masses (e.g., solitary fibrous tumor/hemangiopericytoma, dural metastasis, and lymphoma) were not included in this study, given the fact that these entities tend to be rarer compared to meningioma and schwannoma.

Conclusions

Histogram analyses of diffusion parameters derived from QSI and DWI were both useful in differentiating between intracranial meningioma and schwannoma. Our relatively objective ROI placements, which cover the whole-tumor region, were effective and is likely to be more straightforward to place.

Compliance with ethical standards

Conflict of interest Kei Yamada received research grants from Mediphysics, Doctor Net, FUJIFILM, and Daiichi Sankyo.

References

1. Voss NF, Vrionis FD, Heilman CB, Robertson JH. Meningiomas of the cerebellopontine angle. Surg Neurol. 2000;53:439–47.
2. Sweeney AD, Carlson ML, Ehtesham M, Thompson RC, Haynes DS. Surgical approaches for vestibular schwannoma. Curr Otorhinolaryngol Rep. 2014;2:256–64.
3. Yoshino M, Kin T, Nakatomi H, Oyama H, Saito N. Presurgical planning of feeder resection with realistic three-dimensional virtual operation field in patient with cerebellopontine angle meningioma. Acta Neurochir. 2013;155:1391–9.
4. Agarwal V, Babu R, Grier J, Adogwa O, Back A, Friedman AH, et al. Cerebellopontine angle meningiomas: postoperative outcomes in a modern cohort. Neurosurg Focus. 2013;35:E10.
5. Bonneville F, Savatovsky J, Chiras J. Imaging of cerebellopontine angle lesions: an update Part 1: enhancing extra-axial lesions. Eur Radiol. 2007;17:2472–82.
6. Drevelegas A. Extra-axial brain tumors. Eur Radiol. 2005;15:453–67.
7. Asaoka K, Barrs DM, Sampson JH, McElveen JT, Tucci DL, Fukushima T. Intracanalicular meningioma mimicking vestibular schwannoma. Am J Neuroradiol. 2002;23:1493–6.
8. Guermazi A, Lafitte F, Miaux Y, Adem C, Bonneville J-F, Chiras J. The dural tail sign–beyond meningioma. Clin Radiol. 2005;60:171–88.
9. Hallinan JTPD, Hegde AN, Lim WEH. Dilemmas and diagnostic difficulties in meningioma. Clin Radiol. 2013;68:837–44.
10. Yamasaki F, Kurisu K, Satoh K, Arita K, Sugiyama K, Ohtaki M, et al. Apparent diffusion coefficient of human brain tumors at MR imaging. Radiology. 2005;235:985–91.
11. Pavlisa G, Rados M, Pazanin L, Padovan RS, Ozretic D, Pavlisa G. Characteristics of typical and atypical meningiomas on ADC maps with respect to schwannomas. J Clin Imaging. 2008;32:22–7.
12. Xu X-Q, Li Y, Hong X-N, Wu F-Y, Shi H-B. Radiological indeterminate vestibular schwannoma and meningioma in cerebellopontine angle area: differentiating using whole-tumor histogram analysis of apparent diffusion coefficient. Int. J. Neurosci. 2017;127:183–90.
13. Cohen Y, Assaf Y. High b-value q-space analyzed diffusion-weighted MRS and MRI in neuronal tissues - a technical review. NMR Biomed. 2002;15:516–42.
14. Hori M, Fukunaga I, Masutani Y, Taoka T, Kamagata K, Suzuki Y, et al. Visualizing non-Gaussian diffusion: clinical application of q-space imaging and diffusional kurtosis imaging of the brain and spine. Magn Reson Med Sci. 2012;11:221–33.
15. Assaf Y, Ben-Bashat D, Chapman J, Peled S, Biton IE, Kafri M, et al. High b-value q-space analyzed diffusion-weighted MRI: application to multiple sclerosis. Magn Reson Med. 2002;47:115–26.
16. Hori M, Motosugi U, Fatima Z, Kumagai H, Ikenaga S, Ishigame K, et al. A comparison of mean displacement values using high b-value Q-space diffusion-weighted MRI with conventional apparent diffusion coefficients in patients with stroke. Acad Radiol. 2011;18:837–41.
17. Mayzel-Oreg O, Assaf Y, Gigi A, Ben-Bashat D, Verchovsky R, Mordohovitch M, et al. High b-value diffusion imaging of dementia: application to vascular dementia and alzheimer disease. J Neurol Sci. 2007;257:105–13.
18. Yamada K, Sakai K, Akazawa K, Sugimoto N, Nakagawa M, Mizuno T. Detection of early neuronal damage in CADASIL patients by q-space MR imaging. Neuroradiology. 2013;55:283–90.
19. Taylor EN, Ding Y, Zhu S, Cheah E, Alexander P, Lin L, et al. Association between tumor architecture derived from generalized Q-space MRI and survival in glioblastoma. Oncotarget. 2017;8:41815–266.
20. Fatima Z, Motosugi U, Waqar AB, Hori M, Ishigame K, Oishi N, et al. Associations among q-space MRI, diffusion-weighted MRI and histopathological parameters in meningiomas. Eur Radiol. 2013;23:2258–63.
21. Hori M, Motosug U, Fatima Z, Ishigame K, Araki T. Mean displacement map of spine and spinal cord disorders using high b-value q-space imaging-feasibility study. Acta Radiol. 2011;52:1155–8.
22. Peeters F, Rommel D, Abarca-Quinones J, Grégoire V, Duprez T. Early (72-Hour) detection of radiotherapy-induced changes in an experimental tumor model using diffusion-weighted imaging, diffusion tensor imaging, and Q-space imaging parameters: a comparative study. J Magn Reson Imaging. 2011;35:409–17.
23. Just N. Improving tumour heterogeneity MRI assessment with histograms. Br J Cancer. 2014;111:2205–13.
24. Law M, Young R, Babb J, Pollack E, Johnson G. Histogram analysis versus region of interest analysis of dynamic susceptibility contrast perfusion MR imaging data in the grading of cerebral gliomas. Am J Neuroradiol. 2007;28:761–6.
25. Assaf Y, Mayzel-Oreg O, Gigi A, Ben-Bashat D, Mordohovitch M, Verchovsky R, et al. High b value q-space-analyzed diffusion MRI in vascular dementia: a preliminary study. J Neurol Sci. 2002;203–204:235–9.
26. Choi YJ, Lee JH, Kim HO, Kim DY, Yoon RG, Cho SH, et al. Histogram analysis of apparent diffusion coefficients for occult tonsil

cancer in patients with cervical nodal metastasis from an unknown primary site at presentation. Radiology. 2016;278:146–55.
27. Hajian-Tilaki K. Receiver operating characteristic (ROC) curve analysis for medical diagnostic test evaluation. Casp J Intern Med. 2013;4:627–35.
28. DeLong ER, DeLong DM, Clarke-Pearson DL. Comparing the areas under two or more correlated receiver operating characteristic curves: a nonparametric approach. Biometrics. 1988;44:837–45.
29. Kanda Y. Investigation of the freely available easy-to-use software for medical statistics. Bone Marrow Transpl. 2012;48:452–8.
30. Wagner MW, Narayan AK, Bosemani T, Huisman TAGM, Poretti A. Histogram analysis of diffusion tensor imaging parameters in pediatric cerebellar tumors. J Neuroimaging. 2016;26:360–5.
31. Choi YS, Ahn SS, Kim DW, Chang JH, Kang S-G, Kim EH, et al. Incremental prognostic value of ADC histogram analysis over MGMT promoter methylation status in patients with glioblastoma. Radiology. 2016;281(1):175–84.
32. Kang Y, Choi SH, Kim Y-J, Kim KG, Sohn C-H, Kim J-H, et al. Gliomas: histogram analysis of apparent diffusion coefficient maps with standard- or high-b-value diffusion-weighted MR Imaging—correlation with tumor grade. Radiology. 2011;261:882–90.
33. Sakai K, Yamada K, Akazawa K, et al. Can we shorten the q-space imaging to make it clinically feasible? Jpn J Radiol. 2016;35:16–24. https://doi.org/10.1007/s11604-016-0593-8.